3D ULTRASONIC OBJECT DETECTIONS WITH >1 METER RANGE

Zhichun Shao[1], Yande Peng[1*], Sedat Pala[1], Yue Liang[1], and Liwei Lin[1]*
[1]Berkeley Sensor and Actuator Center, Berkeley, California, USA
[*]These authors contribute equally

2021 IEEE 34th International Conference on Micro Electro Mechanical Systems (MEMS) | 978-1-6654-1912-3/20/$31.00 ©2021 IEEE | DOI: 10.1109/MEMS51782.2021.9375173

ABSTRACT

This paper reports an ultrasonic 3D object detector with > 1 meter range based on an AlN piezoelectric micromachined ultrasonic transducers (pMUTs) chip. Compared with the state-of-art technologies, three distinctive advancements have been achieved: (1) more than 1-meter in sensing distance enabled by a bimorph dual electrode pMUT design; (2) small form factor (6×6 mm^2) and a more than 135° field of view; (3) capability of real time 3D object detection with up to 125 fps (frames per second) based on the scheme of ultrasound beamforming. As such, this work could open up a new class of miniaturized, low-power, real-time 3D object detections for applications such as drone navigation, machine vision and so on.

KEYWORDS

3D object detection, pMUTs, long range sensing, beamforming, machine vision.

INTRODUCTION

Real-time machine vision has been rapidly progressed in recent years via the usage of sensors together with the development of drastically increased computation power. The emerging intelligent machines and tools, including drones and autonomous vehicles, have the ability to detect and identify surrounding objects through the combination usages of Lidar, Radar, cameras and ultrasound sensors [1, 2]. Lidar generally has a more than 50-meter detection range. However, its weight is usually more than 1kg and the power consumption is higher than 10W [3], which make it unsuitable for power-constrained cases, such as drone navigations. The miniaturized optical cameras have high image resolutions, light weight and small form-factor but suffer from poor night vision and huge on-device computing power to process the massive (Gbytes) image data [3]. Radars have excellent adaptability for different light and weather condition but the high operating frequency (>10GHz) requires high-speed and high power-consumption CMOS circuits [4].

Among these sensors, ultrasound sensor is desirable for power-constrained and space-limited applications due to its low power consumption, small form factor and low operating frequency [4]. Recently, researchers have demonstrated a 3D rangefinder using an array of AlN piezoelectric micromachined ultrasonic transducers (pMUTs) [5], with low power consumption (<1mW), small formfactor (~5mm) and high frame rate (30fps). However, due to limited electro-mechanical coupling of pMUT, the detection range is short, which makes it hard to be used for broad machine vision applications.

Here, we demonstrated an ultrasonic 3D object detector based on a bimorph dual electrode AlN pMUTs array. The bimorph dual electrode design could give a maximum of 400% transmitting performance enhancement and 400% receiving sensitivity improvement comparing to the conventional unimorph single electrode design [6-8]. This prototype pMUTs array consists of 4×4 elements operating at 101 kHz, within a footprint of 6mm by 6mm. The bimorph dual electrode design and low operating frequency enable a more than 1-meter sensing distance. Furthermore, by using an ultrasound receive beamforming imaging algorithm [9], the pMUT chip is capable of real time 3D object detection with up to 125 fps at the 1-meter sensing range. In the meantime, we also achieved a wide field of view of more than 135°. The experimental results show potential applications in 3D object detection for power-constrained space-limited cases, including drone navigation, machine vision and so on.

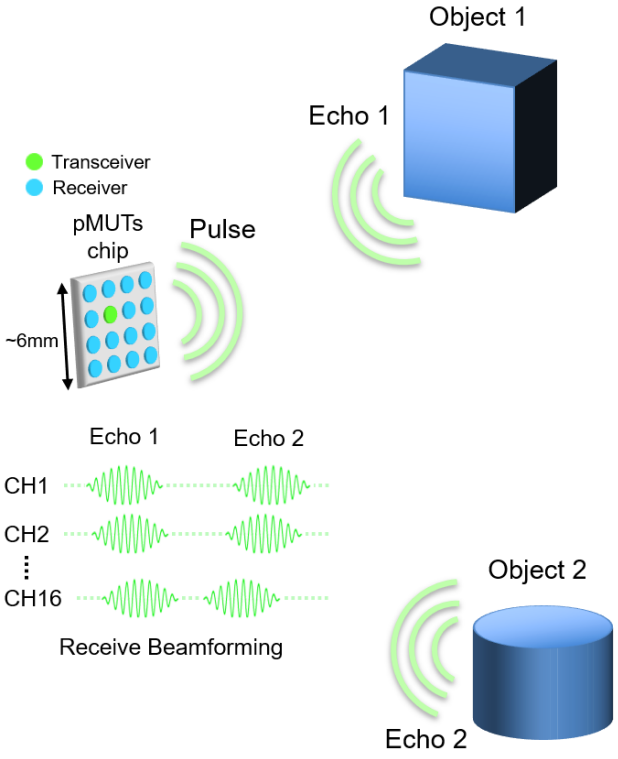

Figure 1, Illustration of the 3D object detection using the scheme of ultrasound receiving beamforming based on a pMUTs array chip.

EXPERIMENTS

Figure 1 illustrates the schematic of the 3D object detection using the ultrasound receiving beamforming scheme based on a pMUTs array. Here, in our ultrasound receive beamforming implementation, only one pMUT element is excited for every pulse transmission event. In the receiving period, all the pMUT elements in the array are used to receive echo signals reflected by the objects. By taking into account the geometrical distance between the transmitting element and all the receiving elements, appropriate phase delay can set the corresponding signals to object locations to compensate for the difference in the Time-of-Flight (ToF). By adding the time-compensated

receiving signals, a 3D image can be reconstructed. Since every transmission event could generate an image, ultrasound receiving beamforming is capable of real time 3D object detection with a high frame rate.

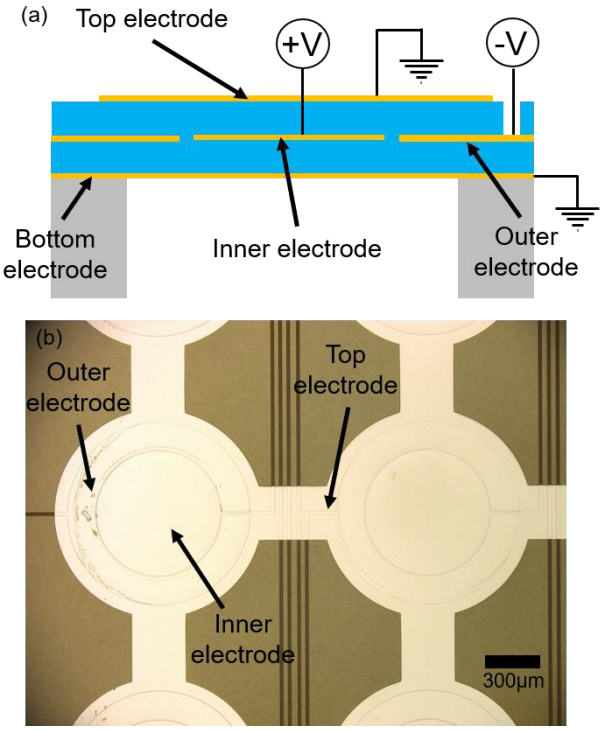

Figure 2, (a) Illustration of the cross-sectional view and (b) microscopic image of a bimorph dual electrode pMUT element.

The design of a bimorph dual electrode pMUT and its operation scheme is illustrated in Figure 2a. By exciting both inner and outer electrodes out-of-phase, a 4-time transmitting performance enhancement can be achieved comparing to that of the conventional unimorph single electrode design [6]. In additional, by differentially reading the received signal from inner and outer electrodes, the receiving sensitivity could be improved by 400%. The bimorph structure consists of two active AlN piezoelectric layers, indicated as blue area in Figure 2a. The thickness of each AlN layer is 1μm. The material of the electrodes is Mo (indicated as yellow area), which has good crystal structure matching with AlN. Figure 2b shows a microscopic image of the fabricated pMUTs array. The radius of the pMUT element is 500 μm, corresponding to a resonant frequency at 101 kHz. The radius of the inner electrode is designed to be 70% of the pMUT diaphragm radius, which is proven to have the optimal output performance [10]. In order to suppress grating lobes [11], the pitch size between pMUT elements is selected to be 1.5 mm, which is close to half of the wavelength ($\lambda/2$ = 1.68 mm) in air at 101 kHz. The detailed fabrication process can be found in the previous work on the bimorph dual-electrode pMUTs [6].

Figure 3 show the scanning electron microscope (SEM) image of the fabricated bimorph dual electrode film stack. Figure 3a displays an SEM image of a suspended AlN diaphragm at the edge of the residual silicon after the backside DRIE process. The residual silicon under the AlN diaphragm is mainly due to the under-etching of silicon in the DRIE process. Figure 3b displays the zoomed in SEM image of the bimorph structure with active AlN layers, Mo electrodes and AlN stop layer. The high crystallinity of AlN layer shown in the SEM images accounts for the high performance of our pMUTs.

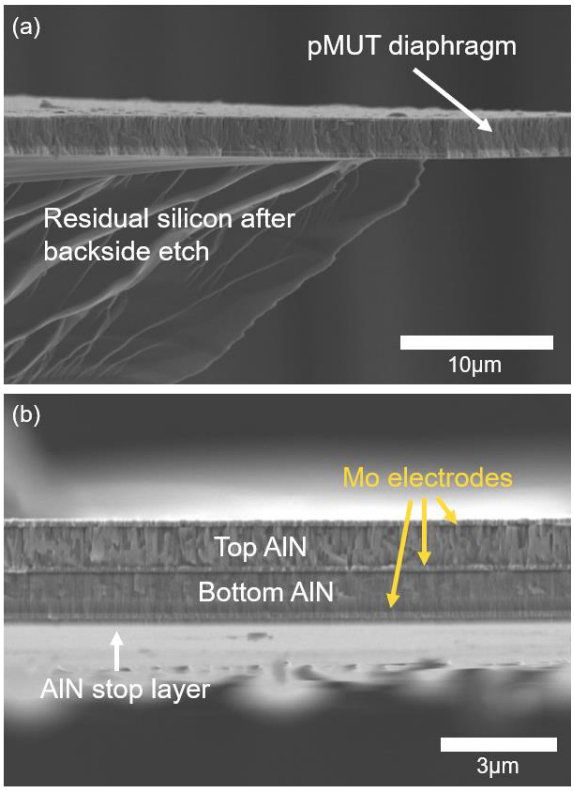

Figure 3,(a) and (b) Scanning electron microscope (SEM) images of the fabricated biomorph dual electrode pMUT film stack.

RESULTS

Figure 4 shows the sound pressure level (SPL) of a bimorph dual electrode pMUT element driving with both inner and outer electrodes. The SPL is measured by a high sensitivity microphone (Bruel & Kjær Type 4138-L-006). Figure 4a displays the frequency response of the device by frequency sweeping. The pMUT element is placed 10 cm away from the microphone. A maximum 91 dB/V SPL is obtained at the 101 kHz resonant frequency. The path loss is measured by varying the distance between the pMUT element and the microphone from 10 cm to 1.1 m as shown in Figure 4b. An out-of-phase $20V_{pp}$ driving signal is applied to inner and outer electrodes at the resonant frequency. The model fitted SPL curve for 101 kHz is also plotted along with the measured results, which shows good accordance with each other. From 1-meter away, an attenuation of only ~20dB is observed with 89dB remaining. The low SPL attenuation in air ensures the imaging performance of the pMUTs chip.

Figure 5a shows the setup for our 3D object detection experiment. A plate is fixed in parallel to the pMUTs chip, which is around 1 meter in height above. Foam absorbers are used to eliminate the undesired echo signal reflected by the box which is used for lifting the iron support. A bowling ball is placed around 50 cm away from the chip

horizontally and about 20 cm in height. These two objects at different angles demonstrate the large field of view (>± 65°) of our pMUT chip. The overall block diagram is illustrated in Figure 5b. A charge amplifier and a low-pass filter is used to amplify and filter the received ultrasound signals. Figure 5c shows the pMUTs array used for both transmitting and receiving, consisting of 4 × 4 elements. During each pulse transmission event, element B2 is used as a transmitter while all the elements are used as receivers during the receiving period. The received signals from different elements are collected by the oscilloscope and post-processed to extract the phase information.

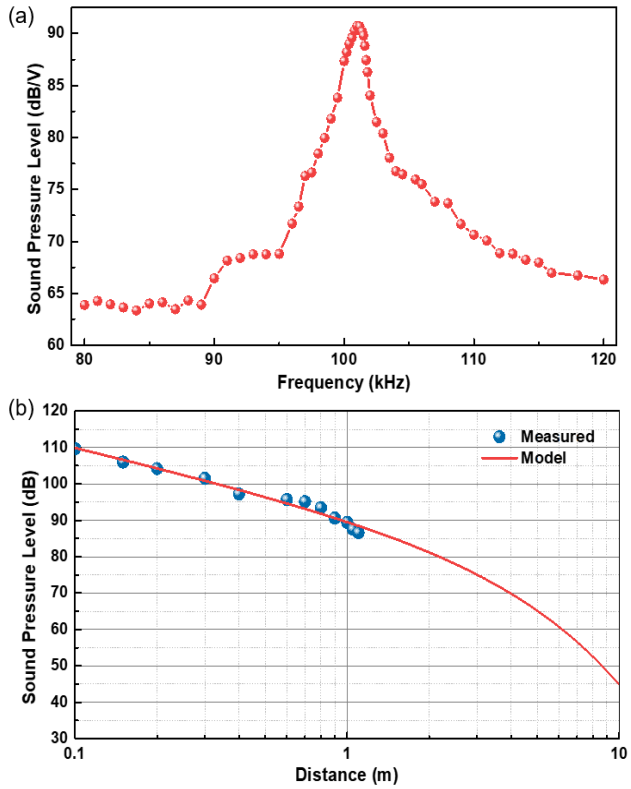

Figure 4, (a) Sound pressure level (SPL) per volt vs. frequency at 10 cm from the pMUT element and (b) SPL vs. distance of the pMUT element driving with both inner and outer electrodes at 20 Vpp.

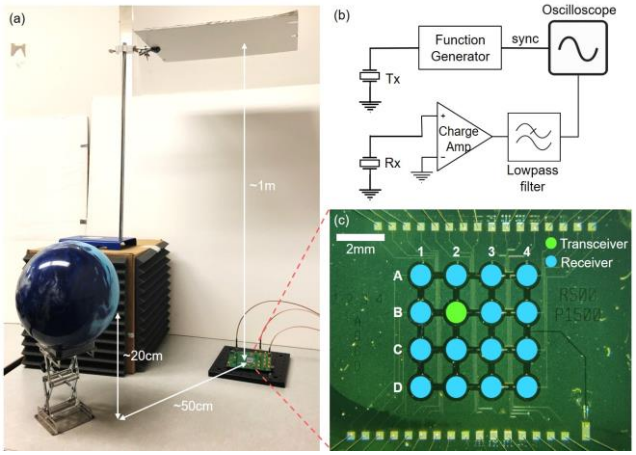

Figure 5, (a) 3D object detection setup; (b) illustration of the overall block diagram for transmission and receiving; (c) an optical image of the pMUTs array.

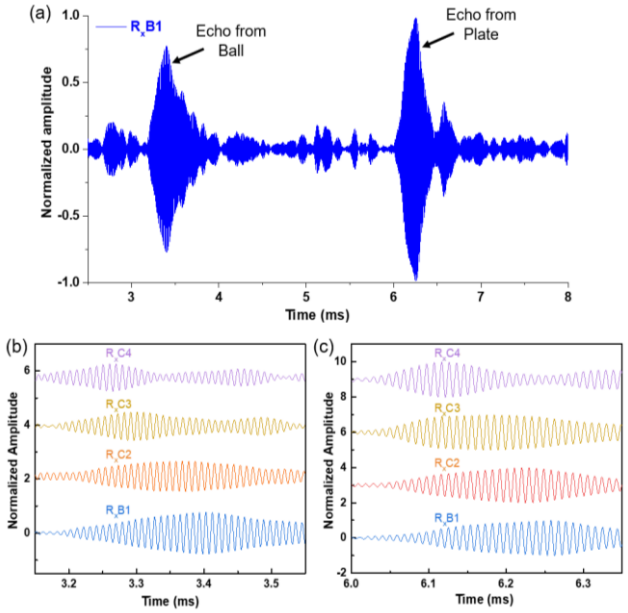

Figure 6, (a) Normalized received echo signals of element B1; zoom-in view of the echo from (b) a ball and (c) a plate of element B1, C2, C3 and C4.

During the transmission event, a 15-cycle 20 Vpp 101 kHz out-of-phase square wave pulse is applied to the inner and outer electrodes of the element B2. The normalized received echo signal of element B1 after digital filtering in MATLAB is plotted in Figure 6(a). The echo from the ball and the plate can be clearly recognized. Figure 6(b) and (c) show the zoom-in view of the echo signals from the ball and the plate of four elements (B1, C2, C3, C4), respectively. Different phase delays corresponding to the spatial location of the objects can be observed in Figures 6(b) and (c). The receiving period is set to be 8 ms, which corresponds to a maximum frame rate of 125 fps.

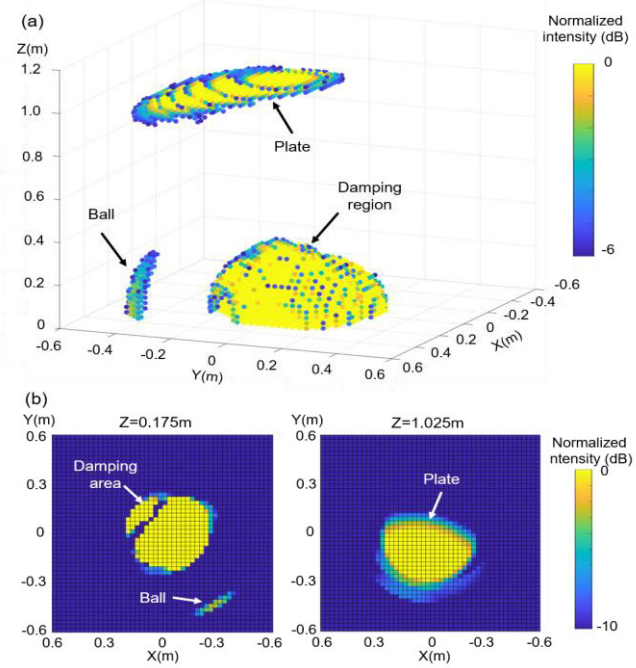

Figure 7, (a) 3D object detection imaging result; reconstructed X-Y plane image at (b) Z=0.175 m and (c) Z=1.025 m.

The 3D imaging results are shown in Figure 7. The image is reconstructed using the DMAS (delay multiply and sum) algorithm [12, 13], which effectively suppresses the level of noise floor comparing to a conventional algorithm such as DAS (delay and sum) [14]. Figure 7(a) displays the 3D object detection result. The locations of the ball and the plate images are in good accordance with the experimental setup. However, the damping and crosstalk signal right after pulse transmission results in a damping region in the reconstructed image, which prevents detecting objects nearby the chip. The single element transmission ensures nearly isotropic radiation, allowing the system to capture the entire field of view in a single transmission event. Figures 7(b) and (c) display the X-Y plane image at height Z=0.175m and Z=1.025m. The imaging results validate the more than 1-meter sensing range and >135° field of view.

CONCLUSION

We demonstrated an ultrasonic 3D object detector based on a bimorph dual electrode AlN pMUTs array. The bimorph dual electrode design could give a maximum of 400% transmitting performance enhancement and 400% receiving sensitivity improvement comparing to those of the conventional unimorph single electrode design. The 4 x 4 pMUTs array operate at 101 kHz, within a footprint of 6mm by 6mm. Based on the 3D object detection results using the scheme of ultrasound receiving beamforming, we achieved a more than 1-meter sensing range and more than 135° field of view, with the capability of real time imaging at a maximum frame rate of 125 fps. As such, the proposed pMUTs chip could open up a new class of miniaturized low-power real-time 3D object detection for drone navigation, machine vision and so on.

ACKNOWLEDGEMENTS

This work was supported in part by BSAC (Berkeley Sensor and Actuator Center, an NSF/Industry/University collaboration center). We thank the insightful discussion with Hirohisa Yabuki. These devices were fabricated at the UC Berkeley Marvell Nanofabrication Lab. Professor Liwei Lin is a core-principal investigator of the Tsinghua-Berkeley Shenzhen Institute (TBSI) and we acknowledge the funding support of TBSI.

REFERENCES

[1] S. Lee, D. Har, and D. Kum, "Drone-assisted disaster management: Finding victims via infrared camera and lidar sensor fusion," in *2016 3rd Asia-Pacific World Congress on Computer Science and Engineering (APWC on CSE)*, 2016: IEEE, pp. 84-89.

[2] Q. Li, L. Chen, M. Li, S.-L. Shaw, and A. Nüchter, "A sensor-fusion drivable-region and lane-detection system for autonomous vehicle navigation in challenging road scenarios," *IEEE Transactions on Vehicular Technology,* vol. 63, no. 2, pp. 540-555, 2013.

[3] N. Jayaweera, N. Rajatheva, and M. Latva-aho, "Autonomous driving without a burden: View from outside with elevated lidar," in *2019 IEEE 89th Vehicular Technology Conference (VTC2019-Spring)*, 2019: IEEE, pp. 1-7.

[4] R. J. Przybyla, H.-Y. Tang, A. Guedes, S. E. Shelton, D. A. Horsley, and B. E. Boser, "3D ultrasonic rangefinder on a chip," *IEEE Journal of Solid-State Circuits,* vol. 50, no. 1, pp. 320-334, 2014.

[5] R. J. Przybyla, H.-Y. Tang, S. E. Shelton, D. A. Horsley, and B. E. Boser, "12.1 3D ultrasonic gesture recognition," in *2014 IEEE International Solid-State Circuits Conference Digest of Technical Papers (ISSCC)*, 2014: IEEE, pp. 210-211.

[6] S. Akhbari, F. Sammoura, B. Eovino, C. Yang, and L. Lin, "Bimorph piezoelectric micromachined ultrasonic transducers," *Journal of Microelectromechanical Systems,* vol. 25, no. 2, pp. 326-336, 2016.

[7] Z. Shao, S. Pala, Y. Liang, T. Jiang, and L. Lin, "Non-Contact Surface Temperature Sensing Based on a Single Bimorph pMUTs Array," in *2020 IEEE 33rd International Conference on Micro Electro Mechanical Systems (MEMS)*, 2020: IEEE, pp. 861-864.

[8] S. Pala, Y. Liang, B. Eovino, Z. Shao, and L. Lin, "Radius of Curvature Measurement Using Piezoelectric Micromachined Ultrasonic Transducers," in *2020 IEEE 33rd International Conference on Micro Electro Mechanical Systems (MEMS)*, 2020: IEEE, pp. 865-868.

[9] L. Demi, "Practical guide to ultrasound beam forming: Beam pattern and image reconstruction analysis," *Applied Sciences,* vol. 8, no. 9, p. 1544, 2018.

[10] F. Sammoura, K. Smyth, and S.-G. Kim, "Optimizing the electrode size of circular bimorph plates with different boundary conditions for maximum deflection of piezoelectric micromachined ultrasonic transducers," *Ultrasonics,* vol. 53, no. 2, pp. 328-334, 2013.

[11] Y. Paul, D. Barthez, R. Léveillé, V. Peter, and D. Scrivani, "Side lobes and grating lobes artifacts in ultrasound imaging," *Veterinary Radiology & Ultrasound,* vol. 38, no. 5, pp. 387-393, 1997.

[12] G. Matrone, A. Ramalli, A. S. Savoia, P. Tortoli, and G. Magenes, "High frame-rate, high resolution ultrasound imaging with multi-line transmission and filtered-delay multiply and sum beamforming," *IEEE transactions on medical imaging,* vol. 36, no. 2, pp. 478-486, 2016.

[13] H. Hu *et al.*, "Stretchable ultrasonic transducer arrays for three-dimensional imaging on complex surfaces," *Science advances,* vol. 4, no. 3, p. eaar3979, 2018.

[14] B. Y. Yiu, I. K. Tsang, and C. Alfred, "GPU-based beamformer: Fast realization of plane wave compounding and synthetic aperture imaging," *IEEE transactions on ultrasonics, ferroelectrics, and frequency control,* vol. 58, no. 8, pp. 1698-1705, 2011.

CONTACT

*Z.Shao, tel: +1-510-220-0974;
zhichun_shao@berkeley.edu